Journal of Materials Chemistry C

PAPER

View Article Online
View Journal | View Issue

Cite this: J. Mater. Chem. C, 2014, 2, 2183

Influence of side chain length and bifurcation point on the crystalline structure and charge transport of diketopyrrolopyrrole-quaterthiophene copolymers (PDQTs)†

Shaoyun Chen,‡[ab] Bin Sun,‡[a] Wei Hong,[a] Hany Aziz,[c] Yuezhong Meng*[b] and Yuning Li*[a]

Received 12th November 2013
Accepted 27th December 2013

DOI: 10.1039/c3tc32219j

www.rsc.org/MaterialsC

The influence of the side chain on the molecular organization and charge transport performance of diketopyrrolopyrrole-quaterthiophene copolymers (PDQTs) was studied. It was found that, by increasing the side chain length from 2-octyldodecyl (**PDQT-20**) to 2-decyltetradecyl (**PDQT-24**), the mobility increased from 2.10 $cm^2\ V^{-1}\ s^{-1}$ up to 3.37 $cm^2\ V^{-1}\ s^{-1}$ in organic thin film transistors (OTFTs). The increase was found to be due to the improved surface morphology, rather than the changes in crystallinity and π–π stacking distance. A new side chain substituent, 4-decylhexadecyl, was developed for studying the effects of the bifurcation point of the branched side chains in comparison with 2-octyldodecyl and 2-decyltetradecyl. The 4-decylhexadecyl substituted PDQT (**PDQT-26**) showed a surge in mobility up to 6.90 $cm^2\ V^{-1}\ s^{-1}$. The remarkably enhanced charge transport performance observed for **PDQT-26** was believed to originate from its much shorter π–π distance (3.68 Å) than those of **PDQT-20** (3.79 Å) and **PDQT-24** (3.86 Å). The improvement was the result of a farther distance of the bifurcation point of 4-decylhexadecyl from the polymer backbone, which could effectively minimize the steric interference of the bulky side chain branches with the backbone to facilitate the co-facial π–π stacking.

Introduction

Printed organic thin film transistors (OTFTs) are of extensive research interest mainly because they can be fabricated using printing technologies on plastic substrates, which have great potential to be used in flexible, low cost, and large area electronics.[1] In the past few years, there have been remarkable improvements in the charge carrier mobility of polymer semiconductors by using push–pull or donor–acceptor (D–A) structures.[2,3] The D–A moiety shortens the intermolecular distance along the co-facial π–π stacking direction, greatly facilitating interchain charge carrier hopping. Diketopyrrolopyrrole (DPP) based D–A polymers represent a class of high performing polymer semiconductors for OTFTs.[3] Many DPP based polymers exhibit mobility greater than 1 $cm^2\ V^{-1}\ s^{-1}$, outperforming amorphous silicon that has a typical mobility range of 0.1–1 $cm^2\ V^{-1}\ s^{-1}$. We reported a simple DPP polymer, PDQT, comprising DPP and β-unsubstituted quaterthiophene (QT), which showed a high hole mobility of ~1 $cm^2\ V^{-1}\ s^{-1}$.[3b] Recently, we demonstrated that a higher mobility value of up to 5.5 $cm^2\ V^{-1}\ s^{-1}$ could be achieved for PDQT through optimization of the purification procedure.[3g] This polymer was also found to be a good donor material for organic photovoltaics (OPVs), reaching a power conversion efficiency as high as 5.62%.[4] Interestingly, PDQT exhibited a mobility value of 2.0×10^{-2} $cm^2\ V^{-1}\ s^{-1}$ along the direction perpendicular to the substrate, determined by the space charge limited current (SCLC) method, which is the highest value reported for donor polymers for OPVs.[5] The high hole mobility of PDQT enabled OPV devices with a very high active layer thickness of up to ~800 nm, which will be very useful for more feasible manufacturing of large area OPV devices *via* high speed roll-to-roll printing processes. Therefore, PDQT is a very promising polymer semiconductor for printed electronics. Recently, it was found that side chain engineering has significant impacts on a number of conjugated polymers[6–10] and small molecules.[11] Side chains with appropriate length were demonstrated to increase the charge carrier mobility significantly, which are accounted for by the improved

[a]*Department of Chemical Engineering and Waterloo Institute for Nanotechnology (WIN), 200 University Ave W, Waterloo, Ontario, N2L 3G1, Canada. E-mail: yuning.li@uwaterloo.ca; Fax: +1-519-888-4347; Tel: +1-519-888-4567 ext. 31105*

[b]*The Key Laboratory of Low-carbon Chemistry & Energy Conservation of Guangdong Province/State Key Laboratory of Optoelectronic Materials and Technologies, Sun Yat-Sen University, Guangzhou 510275, P. R. China. E-mail: mengyzh@mail.sysu.edu.cn*

[c]*Department of Electrical and Computer Engineering/Waterloo Institute for Nanotechnology (WIN), University of Waterloo, 200 University Avenue West, Waterloo, Ontario, N2L 3G1, Canada*

† Electronic supplementary information (ESI) available. See DOI: 10.1039/c3tc32219j

‡ These authors contributed equally.

crystallinity/molecular ordering[6] or shortened π–π stacking distance.[7] Another recent finding is that positioning the bifurcation point of the branched side chains away from the polymer backbone could have noted influences on the charge transport of polymer semiconductors.[8–10] The steric interference of the bulky side chain branches with the co-facial π–π stacking of the conjugated polymer backbone could be minimized by moving away the bifurcation point, leading to dramatically increased mobility.

To further explore the potential of PDQT as an OTFT channel semiconductor, in this study, we investigated the effects of the chain length and the bifurcation point position of branched alkyl side chains on the molecular organization and the charge transport characteristics of this polymer. We found that under the same device fabrication conditions, by increasing the size of the side chain from 2-octyldodecyl to 2-decyltetradecyl, the mobility of PDQT increased from 2.10 $cm^2 V^{-1} s^{-1}$ to 3.37 $cm^2 V^{-1} s^{-1}$. Increasing the distance of the bifurcation point from two carbon atoms (for 2-octyldodecyl) away from the polymer backbone to four carbon atoms (for 4-decylhexadecyl) further significantly improved the mobility up to 6.90 $cm^2 V^{-1} s^{-1}$.

Experimental

Materials

All chemicals were obtained from commercial sources and used as received without further purification. 3,6-Di(thiophen-2-yl)-pyrrolo[3,4-*c*]pyrrole-1,4(2*H*,5*H*)-dione (**DBT-H**),[3g] 3,6-bis(5-bromothiophen-2-yl)-2,5-bis(2-octyldodecyl)pyrrolo[3,4-*c*]pyrrole-1,4(2*H*,5*H*)-dione (**M-20**),[3g] and 3,6-bis(5-bromothiophen-2-yl)-2,5-bis(2-decyltetradecyl)pyrrolo[3,4-*c*]pyrrole-1,4(2*H*,5*H*)-dione (**M-24**)[7] were prepared according to the literature methods.

Synthesis of diethyl 2-(2-decyltetradecyl)malonate (1)

Under argon protection, sodium (1.84 g, 0.08 mol) was reacted with dry ethanol (65 mL) and diethyl malonate (10.57 g, 0.08 mol). After stirring for 1 h at room temperature, 2-decyltetradecyl bromide (33.40 g, 0.08 mol) was added. After refluxing overnight, excess ethanol was evaporated under reduced pressure. The residue was washed with water and extracted with diethyl ether three times. The combined organic phase was dried over anhydrous Na_2SO_4, filtered, and evaporated under reduced pressure. The residue was further purified by column chromatography on silica gel (hexane : ethyl acetate = 20 : 1–10 : 1) to give a colourless liquid, as a mixture of ethyl (~90 mol %) and methyl (~10 mol%) esters. Yield: 29.0 g (73.3%). ^{1}H-NMR ($CDCl_3$, 300 MHz, ppm) δ 4.20 (q, ~3.6H, OCH_2, J = 7.2 Hz), 3.73 (s, ~0.6H, OCH_3), 3.52–3.34 (t, 1H, J = 7.5 Hz). 1.84 (m, 2H), 1.50–1.15 (m, 40H + 1H + ~4.8H, CH_2, CH and OCH$_2CH_3$), 0.88 (t, 6H). ^{13}C-NMR ($CDCl_3$, 75 MHz, ppm) δ 170.48, 169.99, 169.89, 61.49, 61.40, 52.52, 50.29, 50.13, 35.61, 33.32, 33.35, 33.27, 33.20, 32.08, 30.14, 29.84, 29.80, 29.51, 26.46, 22.85, 14.27, 14.24.

Synthesis of 4-decylhexadecanoic acid (2)

A solution of KOH (16.27 g, 0.29 mol) in water (30 mL) was slowly added to a solution of diethyl 2-(2-decyltetradecyl)-malonate (28.82 g, 0.058 mol) in ethanol (62 mL) at room temperature. The reaction mixture was refluxed for 4 h and ethanol was distilled off. Water (300 mL) was added and the mixture was acidified with conc. HCl (~12 N). After phase separation, the combined organic phase was washed with water, dried over anhydrous Na_2SO_4 and filtered. Removal of solvent from the filtrate gave the diacid as a yellow solid, which was heated under reduced pressure at 180 °C until there were no bubbles coming out to afford 4-decylhexadecanoic acid (22.0 g, 95.5%). This product was used in the next step without further purification. ^{1}H-NMR ($CDCl_3$, 300 MHz, ppm) δ 2.33 (t, J = 8.1 Hz, 2H), 1.62 (m, 3H), 1.26 (m, 40H); 0.88 (t, 6H). ^{13}C-NMR ($CDCl_3$, 75 MHz, ppm) δ 179.52, 37.09, 33.39, 32.08, 31.48, 30.20, 29.84, 29.82, 29.51, 28.60, 26.67, 22.58, 14.27.

Synthesis of 4-decylhexadecan-1-ol (3)

To a suspension of 4-decylhexadecanoic acid (21.67 g, 54.6 mmol) in dry diethyl ether (170 mL) was added a $LiAlH_4$ solution (109.2 mmol, 109.2 mL, 1 M in diethyl ether) dropwise at room temperature. The reaction mixture was then refluxed for 12 h before cooling down to room temperature. The mixture was added slowly to water and extracted with diethyl ether three times. The combined organic phase was dried over anhydrous Na_2SO_4 and filtered. Solvent was removed under reduced pressure to give a colourless liquid. Yield: 20.7 g (99.0%). ^{1}H-NMR ($CDCl_3$, 300 MHz, ppm) δ 3.63 (q, J = 6.3 Hz, 2H), 1.65–1.45 (m, 2H), 1.40–1.15 (m, 43H), 0.88 (t, 6H). ^{13}C-NMR ($CDCl_3$, 75 MHz, ppm) δ 63.72, 37.39, 33.75, 32.09, 30.29, 30.13, 29.91, 29.90, 29.88, 29.85, 29.83, 29.72, 29.53, 26.82, 22.85, 14.27.

Synthesis of 4-decyl-1-hexadecyl bromide (4)

To a solution of triphenylphosphine (PPh_3) (13.12 g, 50 mmol) in dichloromethane (CH_2Cl_2) (90 mL) was added dropwise a solution of bromine (7.99 g, 50 mmol) in CH_2Cl_2 (10 mL) at room temperature. After stirring for 1 h, compound **3** (19.14 g, 50 mmol) and pyridine (4 mL, 50 mmol) were added. The mixture was stirred at room temperature overnight before a saturated Na_2SO_3 aqueous solution (6 mL) was added with stirring. The organic phase was separated, dried over anhydrous Na_2SO_4, and filtered. After removal of solvent, the residue was purified by column chromatography on silica gel with hexane to give the title compound as a colourless liquid. Yield: 20.3 g (91.1%). ^{1}H-NMR ($CDCl_3$, 300 MHz, ppm) δ 3.39 (t, J = 6.9 Hz, 2H), 1.89–1.76 (m, 2H), 1.45–1.10 (m, 43H), 0.86 (t, 6H). ^{13}C-NMR ($CDCl_3$, 75 MHz, ppm) δ 37.03, 34.51, 33.70, 32.35, 32.12, 30.35, 30.26, 29.89, 29.86, 29.85, 29.56, 26.80, 22.88, 14.29.

Synthesis of 2,5-bis(4-decylhexadecyl)-3,6-di(thiophen-2-yl)-pyrrolo[3,4-*c*]pyrrole-1,4(2*H*,5*H*)-dione (DBT-26)

To a suspension of **DBT-H** (0.451 g, 1.5 mmol) in anhydrous *N*,*N*-dimethylformamide (DMF) (18 mL) were added potassium carbonate (K_2CO_3) (0.622 g, 4.5 mmol) and 4-decyl-1-hexadecyl bromide (2.01 g, 4.5 mmol). The mixture was stirred at 130 °C for 12 h under argon protection. DMF was then removed under reduced pressure. The residue was washed with water and extracted with CH_2Cl_2. The organic phase was separated, dried

over Na_2SO_4, and filtered. After removal of solvent, the residue was purified by column chromatography on silica gel (CH_2Cl_2 : hexane = 1 : 1) to afford the product. Yield: 0.95 g (61.7%). ^{1}H-NMR ($CDCl_3$, 300 MHz, ppm) δ 8.92 (d, J = 3.6 Hz, 2H), 7.62 (d, J = 4.8 Hz, 2H), 7.29 (d, J = 4.5 Hz, 2H), 1.80–1.60 (m, 4H), 1.45–1.05 (m, 86H), 0.88 (t, 6H). ^{13}C-NMR ($CDCl_3$, 75 MHz, ppm) δ 161.42, 140.10, 135.42, 130.70, 129.91, 128.73, 107.79, 42.68, 37.26, 33.66, 32.07, 30.60, 30.23, 29.86, 29.81, 29.51, 27.18, 26.82, 22.84, 14.27.

Synthesis of 3,6-bis(5-bromothiophen-2-yl)-2,5-bis(4-decylhexadecyl)pyrrolo[3,4-*c*]pyrrole-1,4(2*H*,5*H*)-dione (M-26)

N-Bromosuccinimide (NBS) (0.153 g, 0.86 mmol) was added in small portions into a solution of **DBT-26** (0.422 g, 0.41 mmol) in chloroform (13 mL) at 0 °C. The reaction mixture was protected from light and stirred at room temperature for 20 h. Solvent was evaporated and the residue was purified by column chromatography on silica gel (hexane : CH_2Cl_2 = 1 : 1) to give **M-26**. Yield: 0.37 g (77.1%). ^{1}H-NMR ($CDCl_3$, 300 MHz, ppm) δ 8.69 (d, J = 4.2 Hz, 2H), 7.24 (d, J = 4.2 Hz, 2H), 1.76–1.60 (m, 4H), 1.45–1.10 (m, 86H), 0.88 (t, 6H). ^{13}C-NMR ($CDCl_3$, 75 MHz, ppm) δ 161.10, 139.11, 135.55, 131.78, 131.26, 119.28, 107.91, 42.75, 37.21, 33.65, 32.09, 30.52, 30.25, 39.87, 29.52, 27.17, 26.85, 22.85, 14.28.

Synthesis of PDQT-26

To a 50 mL dry flask was added **M-26** (0.2494 g, 0.21 mmol), 5,5′-bis(trimethylstannyl)bithiophene (0.1033 g, 0.21 mmol) and tri(*o*-tolyl)phosphine (P(*o*-tolyl)$_3$) (5.1 mg, 8 mol%, 0.0168 mmol). Under argon protection, anhydrous chlorobenzene (18 mL) and tris(dibenzylideneacetone)dipalladium(0) ($Pd_2(dba)_3$) (3.9 mg, 2 mol%, 0.0042 mmol) were added. The reaction mixture was stirred at 130 °C for 72 h. After cooling, 2-bromothiophene (0.5 mL) was added and the mixture was stirred at 130 °C for an additional 2 h. After cooling to room temperature, the reaction mixture was poured into methanol (100 mL). After filtration, the obtained solid was subjected to Soxhlet extraction successively with acetone, hexane, and chloroform. Removing solvent from the chloroform fraction gave the product **PDQT-26**. Yield: 250 mg (99.8%). HT-GPC (in 1,2,4-trichlorobenzene at 140 °C): M_n = 62.6 kDa; M_w = 265.2 kDa; M_w/M_n = 4.24.

Synthesis of PDQT-20 (ref. 3*g*)

This polymer was synthesized using **M-20** according to the procedure described for **PDQT-26**. HT-GPC (in 1,2,4-trichlorobenzene at 140 °C): M_n = 40.0 kDa; M_w = 128.8 kDa; M_w/M_n = 3.22.[3g]

Synthesis of PDQT-24

This polymer was synthesized using **M-24** according to the procedure described for **PDQT-26**. HT-GPC (in 1,2,4-trichlorobenzene at 140 °C): M_n = 54.9 kDa; M_w = 171.5 kDa; M_w/M_n = 3.12.

Instrumentation and methods

^{1}H and ^{13}C NMR spectra were acquired on a Bruker DPX 300 MHz spectrometer in $CDCl_3$ and the chemical shifts were referenced to internal tetramethylsilane (TMS, 0 ppm). Thermogravimetric analysis (TGA) and differential scanning calorimetry (DSC) measurements were carried out on a TA Instruments SDT 2960 under nitrogen at a heating rate of 10 °C min^{-1} and TA Instruments DSC Q2000 at a scanning rate of 10 °C min^{-1}, respectively. High-temperature gel-permeation chromatography (HT-GPC) was carried out on a Malvern 350 HT-GPC system at 140 °C using 1,2,4-trichlorobenzene as an eluent and polystyrene as standards. UV-Vis spectra were recorded with polymer solutions in chloroform and polymer films spin-coated onto quartz substrates using a Thermo Scientific Genesys 10 UV spectrometer. Cyclic voltammetry (CV) measurements were conducted on a Digi-Ivy DY2111 Potentiostat under argon with 0.1 M tetrabutylammonium hexafluorophosphate in anhydrous acetonitrile as the electrolyte. A platinum disk electrode coated with a thin layer of polymer was used as the working electrode, Ag/AgCl was used as the reference electrode, and a platinum wire was used as the counter electrode. The HOMO (highest occupied molecular orbital) energy level was calculated using the equation:

$$E_{\mathrm{HOMO}}\ (\mathrm{eV}) = -\left(E_{\mathrm{ox}}^{\mathrm{onset}} - E_{\mathrm{Fc/Fc^+}}^{\mathrm{onset}}\right) - 4.80\ \mathrm{eV},$$

where $E_{\mathrm{ox}}^{\mathrm{onset}}$ and $E_{\mathrm{Fc/Fc^+}}^{\mathrm{onset}}$ are the onset oxidation potentials for the polymer sample and ferrocene relative to the Ag/AgCl electrode, while the value of −4.80 eV is the HOMO energy level of ferrocene.[12] Reflection X-ray diffraction (XRD) patterns were obtained using polymer thin films (~35 nm) spin-coated on dodecyltrichlorosilane (DTS)-modified Si/SiO_2 substrates on a Bruker D8 Advance diffractometer with Cu Kα radiation (λ = 1.5418 Å). Transmission XRD measurements were carried out on a stack of polymer thin films using a Bruker Smart Apex2 CCD with Mo Kα radiation (λ = 0.71073 Å). Atomic force microscopy (AFM) measurements were carried out on a Dimension 3100 Scanning Probe Microscope.

OTFT device fabrication

Bottom-gate, bottom-contact OTFT devices were fabricated on heavily n^{++}-doped silicon wafer with a ~300 nm thermally grown silicon oxide (SiO_2) top layer having a capacitance of ~11 nF cm^{-2}. Gold source and drain patterns were deposited by thermal evaporation on the SiO_2 layer using a conventional lithography technique. Prior to device fabrication, the substrates were subjected to cleaning with air plasma, acetone, and isopropanol, and then modified with dodecyltrichlorosilane (DTS) in toluene (10 mg mL^{-1}) at 60 °C for 20 min. Subsequently the substrates were washed with toluene, and dried under a nitrogen flow. A layer of **PDQT-20**, **PDQT-24** or **PDQT-26** semiconductor film (~35 nm) was deposited on the substrate by spin-coating a 5 mg mL^{-1} polymer solution in 1,1,2,2-tetrachloroethane (TCE) at a speed of 2000 rpm for 90 s. The substrate was then placed on a hotplate at 150 °C or 200 °C for 15 min in a glove box. Then a poly(methyl methacrylate)

(PMMA) solution in butyl acetate (8 wt%) was spin-coated on top of the polymer semiconductor layer at 3000 rpm for 60 s, followed by drying on a hotplate at 80 °C for 30 min in the same glove box. The resulting PMMA encapsulation layer is ~500 nm thick. The devices were characterized in air by using an Agilent 4155C Semiconductor Parameter Analyzer. The carrier mobility in the saturated regime, μ, was calculated from the slope of the $(I_{DS})^{1/2}$ *versus* V_{GS} plot according to the following equation

$$I_{DS} = \mu C_i \frac{W}{2L}(V_{GS} - V_T)^2,$$

where I_{DS} is the drain current, L and W are the channel length (30 μm) and channel width (1000 μm), C_i is the gate dielectric layer capacitance per unit area, and V_{GS} and V_T are the gate voltage and threshold voltage, respectively. V_T was determined from the V_{GS} axis intercept of the linear extrapolation of $(I_{DS})^{1/2} - V_{GS}$ in the saturation regime at $I_{DS} = 0$.

Results and discussion

In this study, we choose three different alkyl side chains, namely, 2-octyldodecyl, 2-decyltetradecyl, and 4-decylhexadecyl, which can be incorporated into the DPP unit by using respective alkyl bromides in the presence of K_2CO_3 in dry DMF (Scheme 1). 2-Octyldodecyl bromide and 2-decyltetradecyl bromide can be readily prepared from the commercial alcohols using bromine and triphenylphosphine (PPh_3). 4-Decyl-1-hexadecyl bromide

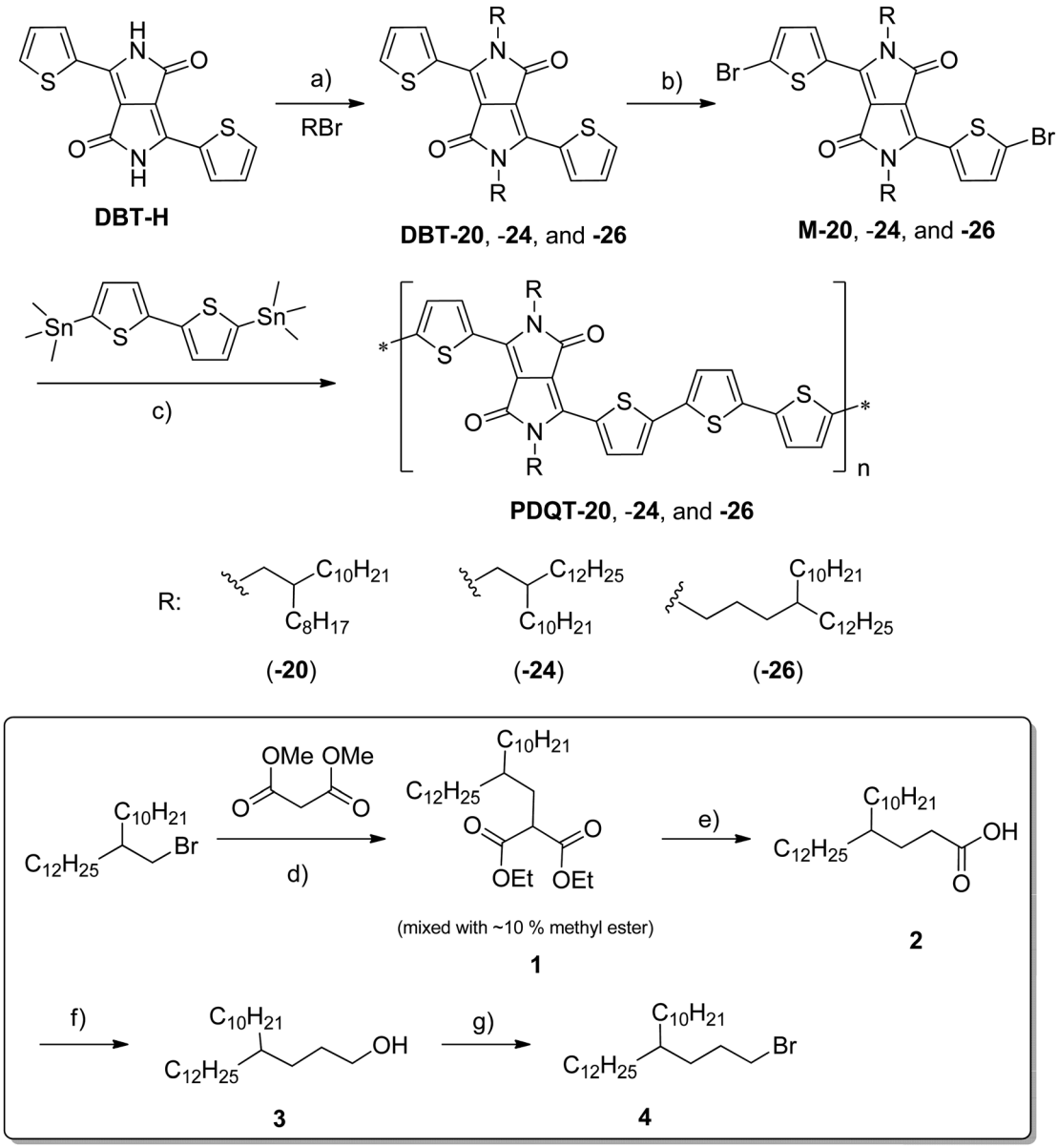

Scheme 1 Synthetic route towards PDQT polymers, **PDQT-20**, **PDQT-24**, and **PDQT-26**: (a) K_2CO_3/DMF/130 °C; (b) NBS/DMF/50 °C; (c) $Pd_2(dba)_3$/P(*o*-tolyl)$_3$/chlorobenzene/130 °C; (d) NaOEt/EtOH/50 °C; (e) (i) KOH/EtOH–H_2O/50 °C, (ii) HCl (conc.), (iii) 180 °C, vacuum; (f) $LiAlH_4$/Et_2O; (g) Br_2/PPh_3/pyridine/CH_2Cl_2/r.t.

Table 1 Optical and electrochemical properties of PDQTs

		λ_{max}^{abs} [a] (nm)		λ_{onset}^{abs} [a] (nm)			Energy levels[e]	
Compounds	M_n (kDa)/PDI	Solution[a]	Film[b]	Film[b]	E_g^{optc} (eV)	E_{ox}^{onsetd} (eV)	E_{HOMO} (eV)	E_{LUMO} (eV)
PDQT-20	40.0/3.22	783	786	932	1.33	0.54	−5.29	−3.96
PDQT-24	54.9/3.12	781	784	939	1.32	0.58	−5.33	−4.02
PDQT-26	62.6/4.24	791	798	954	1.30	0.58	−5.33	−4.03

[a] $\sim 10^{-5}$ M in chloroform. [b] Spin-coated films from chloroform solutions on glass substrates. [c] Calculated from the onset absorption, $E_g^{opt} = 1240/\lambda_{onset}^{abs}$. [d] Calculated using the equation E_{ox}^{onset} (*vs.* Fc/Fc$^+$) = E_{ox}^{onset} (*vs.* Ag/AgCl) − E_{ox}^{onset} (Fc/Fc$^+$ *vs.* Ag/AgCl). [e] Calculated using the equation E_{HOMO} (eV) = $-E_{ox}^{onset}$ (*vs.* Fc/Fc$^+$) − 4.8 eV, $E_{LUMO} = E_{HOMO} + E_g^{opt}$.

(**4**) was synthesized starting from 2-decyltetradecyl bromide according to the procedure outlined in the inset of Scheme 1. The key intermediate carboxylic acid **2** was synthesized using the literature method.[13] **2** was then quantitatively reduced to alcohol **3**, which was subsequently converted to the target bromide **4** using bromine and PPh_3 in the presence of pyridine. The overall yield of four steps from 2-decyltetradecyl bromide to **4** is 67%. The synthetic route towards PDQTs with different alkyl side chains, **PDQT-20**, **PDQT-24**, and **PDQT-26**, is depicted in Scheme 1. The dibromo monomers **M-20**, **M-24**, and **M-26** were conveniently prepared by incorporation of alkyl chains at the nitrogen atoms of the DPP unit using respective alkyl bromides, followed by bromination using *N*-bromosuccinimide (NBS). **M-20**, **M-24**, and **M-26** were then copolymerized with 5,5′-bis-(trimethylstannyl)-2,2′-bithiophene with a catalytic amount of $Pd_2(dba)_3$/P(*o*-tolyl)$_3$ in chlorobenzene to produce **PDQT-20**, **PDQT-24**, and **PDQT-26**, respectively. All polymers were purified extensively using Soxhlet extraction with acetone and hexane to remove oligomers. The remaining polymers were dissolved with chloroform. Molecular weights of all polymers were evaluated by gel permeation chromatography (GPC) with 1,2,4-tricholorobenzene as the eluent at 140 °C (Table 1). All three polymers have high molecular weights with a M_n (the number average molecular weight) of 40.0 kDa, 54.9 kDa and 62.6 kDa for **PDQT-20**, **PDQT-24** and **PDQT-26**, respectively.

These polymers show good thermal stability with the 5% weight loss temperatures ($T_{-5\%}$) of ~395 °C (ESI). **PDQT-20** showed no thermal transition on its differential scanning calorimetric (DSC) curves in the range from −20 °C to 320 °C. On the other hand, **PDQT-24** showed an obvious endothermic peak at 293 °C during the heating sweep and an exothermic peak at 276 °C upon cooling. These results indicate that increasing the size of the side chain from 2-octyldodecylin **PDQT-20** to 2-dodecyltetradecyl in **PDQT-24** could dissociate the polymer chain packing at a much lower temperature due to the easier side chain motion in the latter. Interestingly, **PDQT-26** with an even larger side chain substituent, 4-decylhexadecyl, showed no thermal transition on its DSC profile. This might be due to the lower degree of crystallinity (as confirmed by XRD) or a higher thermal transition temperature of **PDQT-26**.

The UV-Vis absorption spectra of polymers were recorded both in solutions and with thin films. **PDQT-20** showed the wavelength of absorption maximum (λ_{max}) at 783 nm in solution and 786 nm in the solid state, while the λ_{max} of **PDQT-24** blue shifted for 2 nm to 781 nm in solution and to 784 nm in thin film (Fig. 1), suggesting that the bulkier side chains in **PDQT-24** only slightly influenced the conjugation. On the other hand, notable redshifts in absorption were observed for **PDQT-26** that exhibited the λ_{max} at 791 nm in solution and 798 nm in the solid thin film. The UV-Vis data indicate that **PDQT-26** has a more coplanar backbone structure than that of **PDQT-20** and **PDQT-24** in both solution and solid states, which most likely originates from the larger distance of the bifurcation point of the side chain from the backbone in **PDQT-26**.

The electrochemical properties of the polymer thin films were characterized by cyclic voltammetry (CV). Reversible oxidation processes were observed for all three polymers (ESI†). The highest occupied molecular orbital (HOMO) energy levels were calculated from the onset oxidation potentials to be −5.29 eV for **PDQT-20**, −5.33 eV for **PDQT-24**, and −5.33 eV for **PDQT-26**,

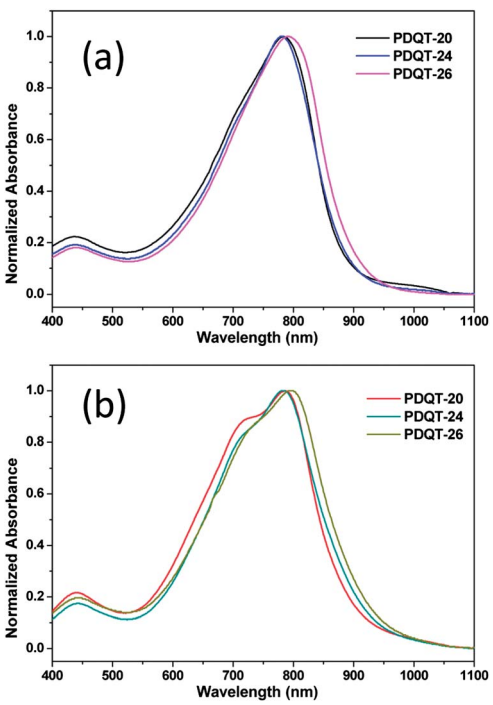

Fig. 1 Normalized UV-Vis absorption spectra of PDQT-20, PDQT-24 and PDQT-26 (a) in $\sim 10^{-5}$ M solutions in chloroform ($CHCl_3$) and (b) as thin films spin-coated from $CHCl_3$ solutions on glass substrates.

which indicated that the position of the bifurcation point of the side chains had little influence on the HOMO energy levels of these polymers. The reduction processes showed significantly lower currents and were less reversible, indicating that these polymers favour hole conduction over electron conduction.

We used reflection and transmission X-ray diffraction (XRD), and atomic force microscopy (AFM) techniques to gain insights into the polymer chain packing and thin film morphologies. Fig. 2a–c show the reflection-mode XRD results of polymer thin films spin-coated on dodecyltrichlorosilane (DTS)-modified SiO_2/Si substrates. For the 150 °C annealed thin films, **PDQT-20** exhibited an intense primary diffraction peak along with higher order peaks up to the 4th order. **PDQT-24** showed a slightly stronger primary peak than that of **PDQT-20**, but the 3rd and 4th order peaks are not observed. **PDQT-26** showed the weakest diffraction peaks, indicating its less ordered layer-by-layer polymer chain packing.

The interlayer *d*-spacing distances of **PDQT-20**, **PDQT-24**, and **PDQT-26** films were calculated using Bragg's law to be 1.94, 2.12 and 2.45 nm, respectively, in good agreement with their increasing side chain length. Since no peaks representing the π–π distance (~3–4 Å) were observed, the polymer chains were likely packed in a lamellar crystalline structure with an edge-on orientation in these thin films.[3b] In order to further substantiate the edge-on molecular orientation in the polymer thin films and elucidate the π–π stacking distance, transmission XRD measurements were carried out on a stack of polymer thin films with a Mo Kα radiation source ($\lambda = 0.71073$ Å). It can be clearly seen in Fig. 2d that the transmission XRD profiles are markedly different from those obtained in the reflection mode. For all polymer samples, the primary peaks corresponding to the interlayer distance are very weak. On the other hand, very strong peaks at $2\theta = \sim 10$–$12°$ were clearly observed. These peaks represent the π–π distances between the polymer chains in the crystalline lamellar domains. The calculated π–π distances are 3.79 Å ($2\theta = 10.78°$) for **PDQT-20**, 3.86 Å ($2\theta = 10.58°$) for **PDQT-24**, and 3.68 Å ($2\theta = 11.08°$) for **PDQT-26**. The results indicate that increasing the side chain length weakens intermolecular π–π interaction of polymers (**PDQT-24** *vs.* **PDQT-20**), while positioning the bifurcation point of the side chain farther from the backbone can dramatically facilitate the π–π stacking due to the reduced steric effect (**PDQT-26** *vs.* **PDQT-24**). The morphology of polymer thin films with increasing annealing temperature was visualized under an atomic force microscope (AFM) (Fig. 3). A rough surface comprising clearly defined grains can be seen in the 150 °C annealed **PDQT-20** thin film. On other hand, the **PDQT-24** and **PDQT-26** films are much smoother and contain very small grains. Increasing the annealing temperature to 200 °C had insignificant effects on the surface morphology of all three polymers.

These polymers were tested as channel semiconductors in bottom-gate, bottom-contact OTFT devices constructed on SiO_2/Si wafer substrates. A polymer solution was spin coated on the substrate with pre-patterned gold source–drain electrode pairs and annealed at 150 °C or 200 °C in a glove box under nitrogen. The devices were encapsulated with ~500 nm of PMMA by spin-coating a PMMA solution in butyl acetate and dried at 80 °C on a hotplate. The devices were characterized in air using an Agilent 4155C *I–V* source measurement unit. All devices showed p-channel charge transport characteristics (Fig. 4 and Table 2). The average (and maximum) mobilities of the polymer films annealed at 150 °C were 1.58 $cm^2 V^{-1} s^{-1}$ (2.10 $cm^2 V^{-1} s^{-1}$) for **PDQT-20**, 2.65 $cm^2 V^{-1} s^{-1}$ (3.37 $cm^2 V^{-1} s^{-1}$) for **PDQT-24**, and 5.18 $cm^2 V^{-1} s^{-1}$ (6.90 $cm^2 V^{-1} s^{-1}$) for **PDQT-26**. The increase in mobility of **PDQT-24** compared with **PDQT-20** is considered a result of the more interconnected grains of the former that facilitates the charge hopping across the polymer thin films. Since **PDQT-26** has the lowest crystallinity among three polymers and the morphologies of **PDQT-26** and **PDQT-24** are very similar, the significantly improved mobility observed for **PDQT-26** is most likely attributable to its higher backbone coplanarity

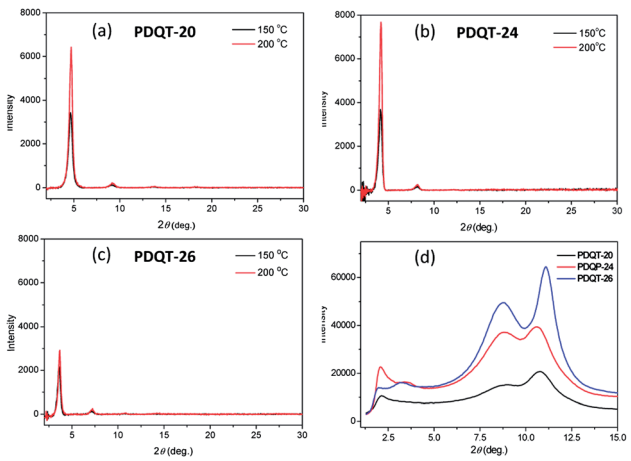

Fig. 2 Reflection XRD diagrams (a–c) of spin coated **PDQT-20**, **PDQT-24** and **PDQT-26** thin films (~35 nm) on a dodecyltrichlorosilane (DTS)-modified SiO_2/Si substrate annealed at different temperatures and transmission XRD diagrams obtained with Cu Kα radiation ($\lambda = 1.5406$ Å) (d) of **PDQT-20**, **PDQT-24** and **PDQT-26** thin film stacks (non-annealed) obtained with Mo Kα radiation ($\lambda = 0.71073$ Å).

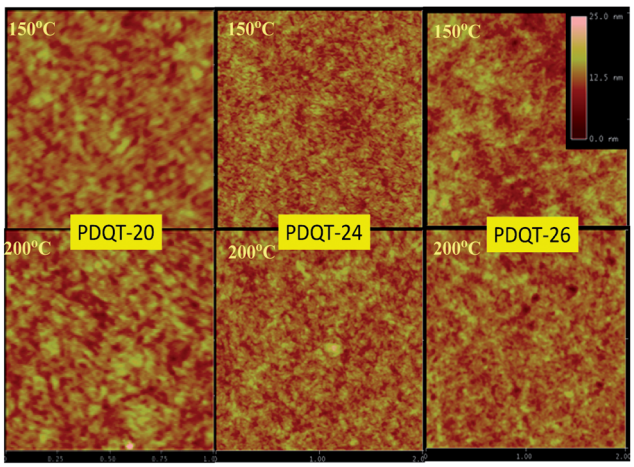

Fig. 3 Height AFM images (2 μm × 2 μm) of spin coated **PDQT-20**, **PDQT-24** and **PDQT-26** thin films (~35 nm) on the DTS-modified SiO_2/Si substrate annealed at different temperatures.

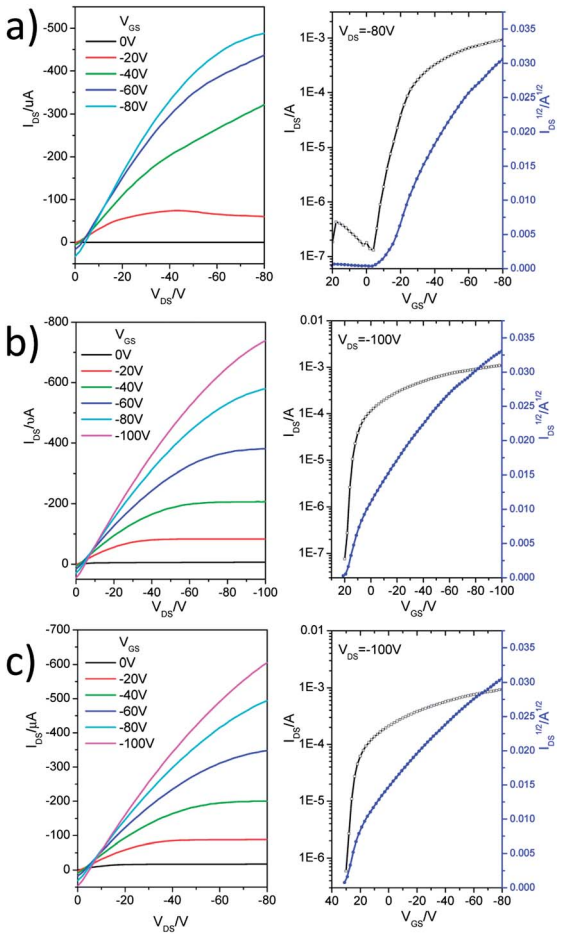

Fig. 4 Output (left) and transfer (right) characteristics of OTFT devices using 150 °C annealed thin films of (a) **PDQT-20** (μ_h = 2.10 cm^2 V^{-1} s^{-1}),[3g] (b) **PDQT-24** (μ_h = 3.37 cm^2 V^{-1} s^{-1}), and (c) **PDQT-26** (μ_h = 6.90 cm^2 V^{-1} s^{-1}). Device dimensions: L = 30 μm; W = 1 mm.

and shorter π–π distance brought about by the more distant bifurcation point of the side chains from the polymer backbone.

The highest mobility achieved for the 150 °C annealed **PDQT-26** films is 6.90 cm^2 V^{-1} s^{-1}, which is among the best mobility values reported so far for polymer semiconductors. OTFT devices with polymer thin films annealed at 200 °C were also evaluated. The average mobility of **PDQT-20** improved to 3.57 cm^2 V^{-1} s^{-1} with the highest value of 5.50 cm^2 V^{-1} s^{-1} due to the increased crystallinity and improved molecular ordering of the polymer thin films at this annealing temperature. However, decreased performance was observed for both **PDQT-24** and **PDQT-26** at this annealing temperature although both polymers showed improved crystallinity. This might be due to the deteriorated polymer/dielectric interfacial contact caused by their more mobile side chains.[14]

Table 2 OTFT device performance of the polymers at different annealing temperatures

Polymer	Annealing temperature (°C)	μ_h[a] (cm^2 V^{-1} s^{-1}) average (max.)	V_T (V)[b]	I_{on}/I_{off}[c]
PDQT-20	150	1.58 (2.10)	−10.0	7.4 × 10^3
(ref. 3*g*)	200	3.57 (5.50)	−6.8	1.4 × 10^6
PDQT-24	150	2.65 (3.37)	18.2	2.6 × 10^4
	200	1.46 (1.51)	17.6	1.6 × 10^4
PDQT-26	150	5.18 (6.90)	27.1	1.6 × 10^4
	200	1.52 (1.55)	13.5	2.9 × 10^3

[a] The average (maximum) mobility value calculated from the saturation region at a drain–source voltage (V_{DS}) of −100 V. [b] The average threshold voltage. [c] The average current on/off ratio.

Conclusions

The effects of the side chain length and bifurcation point position on the molecular organization and charge transport properties of a series of diketopyrrolopyrrole-quaterthiophene polymers (PDQTs) in OTFTs were investigated. A comparative study of PDQTs substituted with 2-octyldodecyl (**PDQT-20**), 2-decyltetradecyl (**PDQT-24**), and 4-decylhexadecyl (**PDQT-26**) was conducted. It was found that **PDQT-24** that has longer side chains showed a much improved mobility of up to 3.37 cm^2 V^{-1} s^{-1} compared to that of **PDQT-20** (2.10 cm^2 V^{-1} s^{-1}) in OTFT devices annealed at 150 °C. The crystallinity of **PDQT-24** was found to be similar to **PDQT-20**, which did not contribute to the improved performance of the former. The π–π distance of **PDQT-24** (3.86 Å) increased with respect to that of **PDQT-20** (3.79 Å), which also had no benefit to the increase in mobility. Therefore, the better performance of **PDQT-24** was considered to be due to its smoother surface morphology and better interconnected networks for more efficient charge transport between grains. **PDQT-26** showed a remarkable increase in mobility up to 6.90 cm^2 V^{-1} s^{-1} in comparison with **PDQT-24** and **PDQT-20**, even though **PDQT-26** thin films showed lower crystallinity than that of both **PDQT-20** and **PDQT-24**. The main reason for this surge in the mobility of **PDQT-26** most likely originates from its much shorter π–π distance (3.68 Å). Our results demonstrated that 4-decylhexadecyl is a very effective new substituent group for polymer semiconductors to enhance the charge transport performance by increasing the main chain coplanarity and shortening the π–π distance.

Acknowledgements

The authors thank the Natural Sciences and Engineering Research Council (NSERC) of Canada for financial support (Discovery Grants and NSERC-DALSA Industry Research Chair Program) of this work. The authors also thank Angstrom Engineering Inc. for providing the thermal deposition system for the fabrication of OTFT devices and Jon Hollinger and Prof. Dwight Seferos of University of Toronto for measuring molecular weights using HT-GPC. SC thanks the Oversea Study Program of Guangzhou Elite Project provided by Guangzhou City, China.

Notes and references

1 (*a*) C. Wang, H. Dong, W. Hu, Y. Liu and D. Zhu, *Chem. Rev.*, 2012, **112**, 2208; (*b*) A. C. Arias, J. D. MacKenzie, I. McCulloch, J. Rivnay and A. Salleo, *Chem. Rev.*, 2010, **110**, 3; (*c*) H. Klauk, *Chem. Soc. Rev.*, 2010, **39**, 2643; (*d*) Y. Wen and Y. Liu, *Adv.*

Mater., 2010, **22**, 1331; (*e*) Y. Wen, Y. Liu, Y. Guo, G. Yu and W. Hu, *Chem. Rev.*, 2011, **111**, 3358; (*f*) P. M. Beaujuge and J. M. J. Fréchet, *J. Am. Chem. Soc.*, 2011, **133**, 20009; (*g*) M. Singh, H. M. Haverinen, P. Dhagat and G. E. Jabbour, *Adv. Mater.*, 2010, **22**, 673; (*h*) A. Facchetti, *Chem. Mater.*, 2011, **23**, 733; (*i*) H. E. Katz and J. Huang, *Annu. Rev. Mater. Res.*, 2009, **39**, 71; (*j*) M. E. Roberts, A. N. Sokolov and Z. Bao, *J. Mater. Chem.*, 2009, **19**, 3351; (*k*) H. Yan, Z. Chen, Y. Zheng, C. Newman, J. R. Quinn, F. Dötz, M. Kastler and A. Facchetti, *Nature*, 2009, **457**, 679.

2 (*a*) C. Guo, W. Hong, H. Aziz and Y. Li, *Rev. Adv. Sci. Eng.*, 2012, **1**, 200; (*b*) L. Biniek, B. C. Schroeder, C. B. Nielsen and I. McCulloch, *J. Mater. Chem.*, 2012, **22**, 14803; (*c*) T. Lei, Y. Cao, Y. Fan, C.-J. Liu, S. C. Yuan and J. Pei, *J. Am. Chem. Soc.*, 2011, **133**, 6099; (*d*) T. Lei, J.-H. Dou, Z.-J. Ma, C.-H. Yao, C.-J. Liu, J.-Y. Wang and J. Pei, *J. Am. Chem. Soc.*, 2012, **134**, 20025; (*e*) H. N. Tsao, D. Cho, J. W. Andreasen, A. Rouhanipour, D. W. Breiby, W. Pisula and K. Müllen, *Adv. Mater.*, 2009, **21**, 209; (*f*) H. N. Tsao, D. M. Cho, I. Park, M. R. Hansen, A. Mavrinskiy, D. Y. Yoon, R. Graf, W. Pisula, H. W. Spiess and K. Müllen, *J. Am. Chem. Soc.*, 2011, **133**, 2605; (*g*) J. R. Matthews, W. Niu, A. Tandia, A. L. Wallace, J. Hu, W.-Y. Lee, G. Giri, S. C. B. Mannsfeld, Y. Xie, S. Cai, H. H. Fong, Z. Bao and M. He, *Chem. Mater.*, 2013, **25**, 782.

3 (*a*) Y. Li, S. P. Singh and P. Sonar, *Adv. Mater.*, 2010, **22**, 4862; (*b*) Y. Li, P. Sonar, S. P. Singh, M. S. Soh, M. Meurs and J. Tan, *J. Am. Chem. Soc.*, 2011, **133**, 2198; (*c*) C. B. Nielsen, M. Turbiez and I. McCulloch, *Adv. Mater.*, 2013, **25**, 1859; (*d*) Y. Li, P. Sonar, S. P. Singh, Z. Zeng and M. S. Soh, *J. Mater. Chem.*, 2011, **21**, 10829; (*e*) Y. Li, P. Sonar, L. Murphy and W. Hong, *Energy Environ. Sci.*, 2013, **6**, 1684; (*f*) H. Lin, W. Lee and W. Chen, *J. Mater. Chem.*, 2012, **22**, 2120; (*g*) B. Sun, W. Hong, H. Aziz, N. M. Abukhdeir and Y. Li, *J. Mater. Chem. C*, 2013, **1**, 4423; (*h*) P. Sonar, S. P. Singh, Y. Li, Z.-E. Ooi, T. Ha, I. Wong, M. S. Soh and A. Dodabalapur, *Energy Environ. Sci.*, 2011, **4**, 2288; (*i*) J. D. Yuen, J. Fan, J. Seifter, B. Lim, R. Hufschmid, A. J. Heeger and F. Wudl, *J. Am. Chem. Soc.*, 2011, **133**, 20799; (*j*) J. S. Ha, K. H. Kim and D. H. Choi, *J. Am. Chem. Soc.*, 2011, **133**, 10364.

4 F. Liu, Y. Gu, C. Wang, W. Zhao, D. Chen, A. L. Briseno and T. P. Russell, *Adv. Mater.*, 2012, **24**, 3947.

5 L. Murphy, W. Hong, H. Aziz and Y. Li, *Sol. Energy Mater. Sol. Cells*, 2013, **114**, 71.

6 J. S. Lee, S. K. Son, S. Song, H. Kim, D. R. Lee, K. Kim, M. J. Ko, D. H. Choi, B. S. Kim and J. H. Cho, *Chem. Mater.*, 2012, **24**, 1316.

7 H. Chen, Y. Guo, G. Yu, Y. Zhao, J. Zhang, D. Gao, H. Liu and Y. Liu, *Adv. Mater.*, 2012, **24**, 4618.

8 J. Mei, D. H. Kim, A. L. Ayzner, M. F. Toney and Z. Bao, *J. Am. Chem. Soc.*, 2011, **133**, 20130.

9 (*a*) J. Lee, A.-R. Han, J. Kim, Y. Kim, J. H. Oh and C. Yang, *J. Am. Chem. Soc.*, 2012, **134**, 20713; (*b*) J. Lee, A.-R. Han, H. Yu, T. J. Shin, C. Yang and J. H. Oh, *J. Am. Chem. Soc.*, 2013, **135**, 9540.

10 (*a*) T. Lei, J. H. Dou and J. Pei, *Adv. Mater.*, 2012, **24**, 6457; (*b*) I. Kang, H.-J. Yun, D. S. Chung, S.-K. Kwon and Y.-H. Kim, *J. Am. Chem. Soc.*, 2013, **135**, 14896.

11 F. Zhang, Y. Hu, T. Schuettfort, C. Di, X. Gao, C. R. McNeill, L. Thomsen, S. C. B. Mannsfeld, W. Yuan, H. Sirringhaus and D. Zhu, *J. Am. Chem. Soc.*, 2013, **135**, 2338.

12 S. Datta, S. R. Forrest, P. Djurovich, E. Polikarpov and M. E. Thompson, *Org. Electron.*, 2005, **6**, 11.

13 Y. P. Liu, D. C. Yin, H. T. Chen and B. G. Sun, *Int. J. Mol. Sci.*, 2010, **11**, 4165.

14 Y. Li, B. Sun, P. Sonar and S. P. Singh, *Org. Electron.*, 2012, **13**, 1606.

